Turkish Journal of Chemistry

Volume 48 | Number 1 Article 8

2-21-2024

Hydroxyl- terminated dendrimers with sulfonimide linkers as binders for metals of industrial significance

Khaleel Abu Sbeih
abusbeih@ahu.edu.jo

Mohammad Al HARAHSHEH
msalharahsheh@just.edu.jo

TÜBİTAK

Turkish Journal of Chemistry

http://journals.tubitak.gov.tr/chem/

Research Article

Turk J Chem
(2024) 48: 85-96
© TÜBİTAK
doi:10.55730/1300-0527.3641

Hydroxyl- terminated dendrimers with sulfonimide linkers as binders for metals of industrial significance

Khaleel ABU SBEIH[1,*], Mohammad AL HARAHSHEH[2]

[1]Department of Chemistry, Faculty of Sciences, Al-Hussein Bin Talal University, Maan, Jordan

[2]Department of Chemical Engineering, Faculty of Engineering, Jordan University of Science and Technology, Irbid, Jordan

Received: 03.06.2023 • **Accepted/Published Online:** 02.01.2024 • **Final Version:** 21.02.2024

Abstract: First- and second-generation hydroxyl- terminated dendrimers were prepared starting from a 1,3-diaminopropane core and sulfonimide linkers. A first-generation mesitylene-derived dendrimer was also prepared with the same terminals. The dendrimers were then reacted with Fe^{3+}, Al^{3+}, and UO_2^{2+} separately in order to apply the dendrimers for binding these metals, which have important industrial applications and pose environmental problems simultaneously. The prepared dendrimers were also shown to bind Fe^{3+} selectively from mixtures with Al^{3+}.

Key words: Hydroxyl- terminated dendrimer, sulfonamide, mesitylene, uranium, aluminum, iron

1. Introduction

Dendrimers are globular compounds with three covalently bonded components: a core, branches, and terminal groups [1]. These nanomaterials, 1–20 nm in diameter, are applied in various fields such as medicine, metal sensing, and catalysis [2]. The dendrimers are used as high-capacity selective binders for metal ions including Pb^{2+}, Cu^{2+}, Fe^{3+}, and Ni^{2+} [2–6]. The use of dendrimers for binding actinides, such as UO_2^{2+} is less known [7,8].

Dendrimers terminated with hydroxyl groups, especially poly(amidoamine) dendrimers (PAMAM-OH) have been used for different purposes, such as removal of heavy metal ions (Cu^{2+}, Ni^{2+}) from water [4], drug delivery [9], therapy [10], and sensing [2,11]. However, the complexation of these dendrimers with the metal ions Al^{3+}, Fe^{3+}, and UO_2^{2+} has been scarce except for Fe^{3+} [7,12-15]. Appelhans et. al. studied the complexation of 3rd-generation poly(propyleneimine) dendrimers (PPI) with maltose shells towards different metal ions (VO^{2+}, Eu^{3+}, and UO_2^{2+}) [12]. Zhou, et. al. used O-binding keto and OH- terminated dendrimers for selective Fe^{3+} binding [15]. Ye et al. studied the uptake of Al^{3+} ions by gallic acid-derivatized dendrimers [14]. Hydroxypyridinone-terminated dendrimers were used by Cusnir et al. to treat Fe overload [13]. Diallo et al. studied UO_2^{2+} binding to PAMAM and PPI dendrimers in aqueous solutions [7].

Sulfonimide- linked dendrimers have attracted increasing attention because they are easily accessible and can be used for different applications [10,16,17]. Moreover, sulfonimide links are environmentally safe. In this article, 1st- and 2nd-generation sulfonimide- based dendrimers L1 and L2, respectively, as well as the easily accessible mesitylene- dendrimer L3 [18], are prepared with hydroxyl terminals derived from tris(hydroxymethyl)aminomethane (tris) in order to bind Al^{3+}, Fe^{3+}, and UO_2^{2+} ions separately and also study the possibility of using these dendrimers for separating iron from aluminum due to their higher affinity toward Fe^{3+} and the lack of reports about using dendrimers for separating Fe from Al.

One of the main methods to extract Al from natural kaolin uses HCl [19]. However, this dissolves Fe leaving the Al solution contaminated with iron. Different methods are used to remove Fe from Al such as solvent extraction which uses phosphates [20], amines [21], and carboxylic acids [22].

The interest in recovering uranium from various sources has increased to meet the growing demand for energy. Moreover, radioactive contamination caused by U is an environmental concern. The most common processes for recovering uranium from minerals such as phosphates are extraction [23], ion exchange [24], and sorption [25]. Organic solvents are hazardous, while exchange processes lack selectivity [24].

Since Al^{3+}, Fe^{3+}, and UO_2^{2+} are hard Lewis acids and thus strongly bind hard bases like O- donors, they are expected to have good affinities for oxygen-terminated dendrimers [26–28]. Therefore, we prepared oxygen-terminated dendrimers

* Correspondence: abusbeih@ahu.edu.jo

for binding these ions. The composition and structures of the dendrimers and their metal complexes were proved by spectroscopic methods as well as elemental and thermal analysis.

2. Materials and methods

All chemicals were purchased off the analytical grade. 4-bromomethylbenzenesulfonyl chloride, 1,3-diaminopropane, 4-nitrobenzene-sulfonyl chloride, and Et_3N from Sigma-Aldrich (USA). All solvents from Tedia (USA). Tris, $FeCl_3$, $AlCl_3$, and K_2CO_3 from Merck (Germany). Uranyl nitrate from BDH (England) and the uranium nitrate standard solution (1000 µg/mL U in 2%–5% aqueous HNO_3) from AccuStandard, (USA).

^{1}H-NMR and ^{13}C-NMR were done on a 400 MHz Bruker instrument using DMSO as a solvent. The infrared spectra were recorded on a Tensor II FT-IR spectrometer with an ATR attachment from Bruker. UV-Vis spectra were recorded using a SPECORD 200 PLUS spectrophotometer, Analytik-Jena (Germany). Elemental analysis was performed using a FLASH 2000 CHNS/O Analyzer, Thermo-Scientific (USA). Thermal gravimetric analysis (TGA) was observed at a rate of 10 °C/min up to 900 °C under N_2 in alumina crucibles using a Netzsch TG 209F1 instrument. The sample mass range was 4.74–13.55 mg.

2.1. Synthesis of L1

Stage 1: 4-bromomethylbenzenesulfonyl chloride (7.0 g, 0.026 mol) was added in small portions to 1,3-diaminopropane (0.321 g, 0.0043 mol) and Et_3N (2.628 g, 0.026 mol) in DCM (100 mL) and the solution refluxed for 2 days. The residue left after evaporation of DCM was stirred in isopropanol for 30 min. This dissolves the impurities leaving a pure solid, Compound 1. Yield: 3.735 g, 87%. M. P., 130 °C. IR (cm^{-1}): 2939, 1474, 1434, 1398, 1171, 1035, 849, 463. ^{1}H-NMR δ (ppm) 7.4–7.9 (Ar, 16H, m), 4.81 ($BrCH_2Ar$, 8H, s), 3.73 (CH_2N, 4H, t), 2.04 (CCH_2C, 2H, m). ^{13}C-NMR δ (ppm) 145.6 (CSO_2), 137.4 (CMe), 130.6 (C-CSO_2), 128.4 (C-CMe), 32.7 (CH_2N), 30.0 ($BrCH_2$), 21.6 (C-CH_2-C).

Stage 2: Compound 1 (2.0 g, 2.0×10^{-3} mol), K_2CO_3 (1.244 g, 9.0×10^{-3} mol), KI (0.15 g), and Tris (1.09 g, 9.0×10^{-3} mol) were added to DMF (120 mL) and stirred at 50 °C for 2 days. The resulting solution was filtered and then evaporated to dryness to afford L1 which was washed with cold ethanol and Et_2O and then dried. Yield: 1.620 g, 70%. Elemental analysis for $C_{47}H_{70}N_6O_{20}S_4$, found (calculated): %C, 48.65 (48.36); %H, 6.12 (6.04); %N, 7.28 (7.20). IR (cm^{-1}): 3335, 3285, 2932, 1594, 1450, 1364, 1296, 1162, 1080, 1037, 855, 768. ^{1}H-NMR δ (ppm) 7.2–7.8 (Ar, 16H, m), 3.69 (OH and NH, 16H, broad), 3.54 (NCH_2Ar, 8H, s), 3.28 (NCH_2O, 24H, m), 2.52 (CH_2NS, 4H, m), 2.34 (CCH_2C, 2H, m). ^{13}C-NMR δ (ppm) 145 (CSO_2), 136 (CMe), 130 (C-CSO_2), 128 (C-CMe), 63 (C-O), 60.4 (*quaternary*-carbon), 57(Ar-CH_2-N), 30.8 (CH_2NAr), 21.01 (C-CH_2-C).

2.2. Synthesis of L2

Stage 1: 4-nitrobenzenesulfonyl chloride (35.864 g, 0.16 mol) was added slowly to a solution of 1,3-diaminopropane (2.0 g, 0.027 mol) and Et_3N (16.376 g, 0.16 mol) in DCM (200 mL). The solution was refluxed for 2 days. The residue left after evaporating DCM was then stirred in methanol (200 mL) for 1 h. This dissolves the impurities leaving a pure solid, Compound 2, which was washed with ethanol and then Et_2O dried. Yield: 17.5 g, 80%. M. P., 238 °C. IR (cm^{-1}): 3032, 1606, 1527, 1475, 1350, 1248, 1162, 1115, 1092, 854, 740, 612. ^{1}H-NMR δ (ppm) 8.28.5 (Ar, 16H, m), 3.91 (CH_2N, 4H, t), 1.99 (CCH_2C, 2H, m). ^{13}C-NMR δ (ppm) 151.3 (CSO_2), 143.8 (CNO_2), 130.1 (C-CSO_2), 125.5 (C-CNO_2), 47.0 (CH_2NAr), 30.7 (C-CH_2-C).

Stage 2: Compound 2 (1.94 g, 2.4×10^{-3} mol) was reduced with $SnCl_2$ (6.441 g, 0.034 mol) in the presence of 0.85 g of 37% HCl in refluxing ethanol (80 mL) for 2 days. The solution was then neutralized with K_2CO_3 and the solids filtered off. The filtrate was evaporated to afford Compound 3 which was crystallized from methanol and then washed with Et_2O. Yield: 1.25 g, 74%. M. P., 190 °C. IR (cm^{-1}): 3454, 3381, 1631, 1598, 1434, 1306, 1151, 1089, 832, 697. ^{1}H-NMR δ (ppm) 6.6–7.7 (Ar, 16H, m), 3.9 (NH, 8H, broad), 2.6 (CH_2N, 4H), 1.46 (CCH_2C, 2H, m). ^{13}C-NMR δ (ppm) 152.4 (CNH_2), 130.4 (CSO_2), 128.0 (C-CSO_2), 113.2 (C-CNH_2), 40.8 (CH_2NAr), 29.7 (C-CH_2-C).

Stage 3: Compound 3 (1.0 g, 1.42×10^{-3} mol) was reacted with 4-(bromomethyl)-benzenesulfonyl chloride (4.657 g, 0.0173 mol) and Et_3N (1.749 g, 0.0173 mol) in a 50:50 DCM/ACN mixture (200 mL). The solution was refluxed for 2 days then the solvent evaporated and the residue stirred with isopropanol (50 mL) for 30 min. The solution was filtered and the solid crystallized from DMF then washed with ethanol and Et_2O to afford a light brown solid, Compound 4. Yield: 2.55 g, 70%. M. P., 227 °C. IR (cm^{-1}): 3044, 1597, 1444, 1406, 1198, 1137, 1050, 1011, 841, 697. ^{1}H-NMR δ (ppm) 7.1–7.9 (Ar, 48H, m), 4.68 ($BrCH_2$, 16H, s), 2.6 (CH_2N, 4H, m), 1.24 (CCH_2C, 2H, m). ^{13}C-NMR δ (ppm) 111.3 (N-C-C(Ar)), 118.9 (NC(Ar)), 126.0 - 129.8 (other aromatic carbons), 46.3 (CH_2N), 34.8 ($BrCH_2$), 9.0 (C-CH_2-C).

Stage 4: Compound 4 (1.0 g, 3.9×10^{-4} mol), K_2CO_3 (0.431 g, 0.0031 mol), KI (0.05 g), and tris (0.378 g, 0.0031 mol) were added to DMF (100 mL) then stirred at 50 °C for 48 h. Filtering and evaporation afforded L2 which was washed with ethanol and Et_2O. Yield: 0.825 g, 73%. Elemental analysis for $C_{115}H_{150}N_{14}O_{48}S_{12}$, found (calculated): %C, 48.17 (47.94); %H,

5.43 (5.25); %N, 7.05 (6.81). M. P., 240 °C. IR (cm^{-1}): 3420, 3250, 1621, 1429, 1384, 1155, 1114, 1085. ^{1}H-NMR δ (ppm) 7.25-7.75 (Ar, 48H, m), 4.49 (NCH_2Ar, 16H, s), 4.34 (OH, 24H, br, s), 3.72 (NH, 8H, s), 3.36 (CH_2O, 48H, m), 3.23 (CH_2NS, 4H, m), 1.3 (CCH_2C, 2H, m). ^{13}C-NMR δ (ppm) 142.8 (CS), 132.6 (C-CH_2N), 127.6 (C-CS), 126.3 (C-C-CS), 61.7 (CH_2O), 60.6 (*quaternary*-carbon), 52.5 (Ar-CH_2-N), 45.6 ($ArNCH_2$), 8.00 (C-CH_2-C). UV-Vis: λ_{max}, nm, (water) 296 (ε, $M^{-1}cm^{-1}$, 6210).

2.3. Synthesis of L3

L3: K_2CO_3 (4.146 g, 0.03 mol), KI (0.02 g), tris (3.634 g, 0.03 mol), and tris(bromo-methyl)mesitylene (4.0 g, 0.01 mol) were added to DMF (100 mL). The solution was stirred at 50 °C for 48 h then filtered and evaporated to afford L3 which was washed with ethanol, Et_2O, and dried. Yield: 4.0 g, 77%. M. P., 148 °C. Elemental analysis for $C_{24}H_{45}N_3O_9$, found (calculated): %C, 55.71 (55.47); %H, 9.02 (8.73); %N, 8.37 (8.09). IR (cm^{-1}): 3355, 3200, 2943, 1593, 1465, 1346, 1290, 1217, 1158, 1042, 792. ^{1}H-NMR δ (ppm) 4.41 (OH, 9H, br), 3.75 ($ArCH_2N$, 6H, s), 3.47 (CH_2O, 18H, m), 3.36 (NH, 3H, br), 2.38 (CH_3, 9H, s). ^{13}C-NMR δ (ppm) 135.6 (C-CH_2N), 134.9 (C-CH_3), 61.6 (C-O), 60.4 (*quaternary*-carbon), 40.8 (N-CH_2Ar), 15.2 (CH_3).

2.4. Synthesis of the metal complexes

The complexes were synthesized by stirring the metal salt and the dendrimer in 40 mL DMF at 20 °C for 2 h then the solvent evaporated and the solid was washed with ethanol and Et_2O and then dried in a vacuum.

2.4.1 Synthesis of L1 complexes

L1 (0.10 g, 8.6×10^{-5} mol) was reacted with 3.8×10^{-4} mol of the metal salt.

1) L1 was reacted with $FeCl_3.6H_2O$ (0.104 g). Yield: 0.10 g, 55%. Elemental analysis for $C_{59}H_{98}N_{10}O_{24}S_4Fe_4Cl_{12}$, found (calculated): %C, 33.72 (33.61); %H, 4.91 (4.68); %N, 6.86 (6.64). IR (cm^{-1}): 3234, 3191, 3112, 2988, 1630, 1553, 1462, 1403, 1296, 1058, 1037, 595. UV-Vis: λ_{max}, nm, (water) 300 (ε, $M^{-1}cm^{-1}$, 3.16×10^3).

2) L1 was reacted with $AlCl_3.6H_2O$ (0.093 g). Yield: 0.085 g, 50%. Elemental analysis for $C_{59}H_{98}N_{10}O_{24}S_4Al_4Cl_{12}$, found (calculated): %C, 35.41 (35.55); %H, 5.13 (4.96); %N, 7.29 (7.03). IR (cm^{-1}): 3184, 3073, 2981, 1664, 1628, 1551, 1464, 1398, 1375, 1298, 1039, 659, 592. UV-Vis: λ_{max}, nm, (water) 301 (ε, 253).

3) L1 in 15 mL DMF was added to standard $UO_2(NO_3)_2$ (91.7 mL). Yield: 0.11 g, 71%. Elemental analysis for $C_{59}H_{98}N_{18}O_{56}S_4U_4$, found (calculated): %C, 23.60 (23.34); %H, 3.18 (3.25); %N, 8.47 (8.31). IR (cm^{-1}): 3449, 1618, 1525, 1469, 1391, 1300, 1023, 826, 716, 500. UV-Vis: λ_{max}, nm, (water) 300 (ε, 5.75×10^3), 357 (ε, 2.65×10^3), 429 (ε, 811).

2.4.2 Synthesis of L2 complexes

L2 (0.10 g, 3.5×10^{-5} mol) was reacted with 2.8×10^{-4} mol of the metal salt.

1) L2 was reacted with $FeCl_3.6H_2O$ (0.075 g). Yield: 0.082 g, 50%. Elemental analysis for $C_{139}H_{206}N_{22}O_{56}S_{12}Fe_8Cl_{24}$, found (calculated): %C, 35.57 (35.04); %H, 4.20 (4.36); %N, 6.70 (6.47). IR (cm^{-1}): 3390, 3330, 3035, 1635, 1593, 1442, 1189, 1126, 1040, 1015, 853, 820, 700, 571. UV-Vis: λ_{max}, nm, (water) 300 (ε, $M^{-1}cm^{-1}$, 1.43×10^4).

2) L2 was reacted with $AlCl_3.6H_2O$ (0.067 g). Yield: 0.090 g, 68%. Elemental analysis for $C_{139}H_{206}N_{22}O_{56}S_{12}Al_8Cl_{24}$, found (calculated): %C, 37.04 (36.83); %H, 4.63 (4.58); %N, 6.97 (6.80). IR (cm^{-1}): 3432, 3121, 1568, 1541, 1461, 1161, 776. UV-Vis: λ_{max}, nm, (water) 304 (ε, 1.93×10^4).

3) L2 was reacted with $UO_2(NO_3)_2.6H_2O$ (0.140 g). Yield: 0.14 g, 61%. Elemental analysis for $C_{139}H_{206}N_{38}O_{120}S_{12}U_8$, found (calculated): %C, 25.43 (25.22); %H, 3.29 (3.14); %N, 8.31 (8.04). IR (cm^{-1}): 3330, 3185, 1631, 1504, 1384, 1344, 1044, 924, 735, 645, 576. UV-Vis: λ_{max}, nm, (water) 297 (ε, 1.46×10^4), 351 (ε, 7620), 434 (ε, 3510).

2.4.3 Synthesis of L3 complexes

L3 (0.12 g, 2.3×10^{-4} mol) was reacted with 7.0×10^{-4} mol of the metal salt.

1) L3 was reacted with $FeCl_3.6H_2O$ (0.188 g). Yield: 0.18 g, 74%. Elemental analysis for $C_{24}H_{51}N_3O_{12}Fe_3Cl_9$, found (calculated): %C, 27.45 (27.19); %H, 5.02 (4.85); %N, 4.18 (3.964). IR (cm^{-1}): 3405, 2975, 1627, 1580, 1463, 1410, 1380, 1330, 1084, 550. UV-Vis: $\lambda_{max,}$ nm, (water) 301 (ε, $M^{-1}cm^{-1}$, 1.58×10^3).

2) L3 was reacted with $AlCl_3.6H_2O$ (0.168 g). Yield 0.103 g, 50%. Elemental analysis for $C_{24}H_{45}N_3O_9Al_3Cl_9$, found (calculated): %C, 31.28 (31.34); %H, 5.16 (4.93); %N, 4.73 (4.57). IR (cm^{-1}): 3441, 3121, 1457, 1269, 1139, 640, 490. UV-Vis: λ_{max}, nm, (water) 298.5 (ε, 705).

3) L3 was reacted with $UO_2(NO_3)_2.6H_2O$ (0.35 g). Yield: 0.235 g, 60%. Elemental analysis for $C_{24}H_{45}N_9O_{33}U_3$, found (calculated): %C, 17.15 (16.94); %H, 2.90 (2.67); %N, 7.65 (7.41). IR (cm^{-1}): 3342, 3135, 1653, 1561, 1383, 1355, 1066, 927, 899, 532. UV-Vis: λ_{max}, nm, (water) 302 (ε, 1.94×10^3), 382 (ε, 165), 430 (ε, 194).

2.5 Selective binding of iron from aluminum solutions

Three separate solutions of Fe^{3+} and Al^{3+} were prepared in 30 mL water by mixing a dendrimer with 3.8×10^{-4} mol of both $FeCl_3.6H_2O$ (0.104 g) and $AlCl_3.6H_2O$ (0.093 g). The solutions were stirred for 20 h at 20 °C then tested for both metals (see A, B).

Solution 1. Dendrimer added: L1, (0.10 g, 8.6×10^{-5} mol).
Solution 2. Dendrimer added: L2, (0.139 g, 4.75×10^{-5} mol).
Solution 3. Dendrimer added: L3, (0.065 g, 1.25×10^{-4} mol).
Test A) A 10 mL sample of the filtered solution was diluted to 100 mL using 0.002 M NaSCN. The absorbance of the resulting $FeSCN^{2+}$ was measured at 447 nm and the free Fe^{3+} was determined using standard Fe^{3+} solutions.
Test B) To a 1 mL sample of the solution, drops of 6 M NH_3 are added until the solution is basic and Al^{3+} precipitates as $Al(OH)_3$(s). To confirm the presence of Al^{3+}, 3 drops of 0.1% (wt/ V) Aluminon solution are added with shaking. Aluminon, the ammonium salt of aurin tricarboxylic acid, adsorbs onto the surface of $Al(OH)_3$ giving it a pink-red color. The solution was then centrifuged producing a red precipitate.

3. Results and discussion

The dendrimers were prepared by the divergent method. L1 and L2 have 1,3-diaminopropane cores and contain sulfonimide linkers. The 1st-generation dendrimer L1 was derived from 4-toluenesulfonyl chloride while the 2nd-generation dendrimer L2 was derived from 4-nitrobenzenesulfonyl chloride. 4-Bromomethylbenzenesulfonyl was then used to extend the branches. Unlike these two dendrimers, the 1st-generation dendrimer L3 has a mesitylene core. The terminals were derived from tris and act as tridentate ligands to each metal via O atoms. These hard atoms are suited to bind hard metals with high oxidation states such as Al^{3+}, Fe^{3+}, and UO_2^{2+}. The off-white ligands were slightly soluble in the polar solvents water, DMF, and DMSO, and insoluble in Et_2O and benzene reflecting their high polarity. The dendrimers were characterized using IR, ^{1}H-NMR, and ^{13}C-NMR spectroscopy. Elemental analysis confirmed the composition of the ligands.

3.1. Dendrimers derived from 4-toluenesulfonyl chloride, L1

The dendrimer L1 was prepared by reacting 1,3-diaminopropane with excess 4-bromomethyl-benzenesulfonyl chloride, in the presence of Et_3N as a base, resulting in the introduction of four 4-toluenesulfonyl groups on the two nitrogen atoms (Scheme 1). Evidence for full substitution on N comes from the IR data of the dendrimer, Compound 1, which does not show any NH stretching vibrations (Figure S1). The aromatic and sulfonyl vibrations appear at their usual positions and C-Br stretching vibrations appear at 463 cm^{-1} [29]. The tetrabrominated product was then reacted with tris in the presence of K_2CO_3 as a base and KI as a catalyst, causing the disappearance of the C-Br stretching vibration in L1 (Figure S2). Benzene ring vibrations appear at 1594, 1450, and 855 cm^{-1}. Stretching vibrations due to sulfonyl groups give rise to absorptions at 1364 and 1162 cm^{-1}. A broad band at 3335 was assigned to stretching vibrations of the alcoholic OH groups, for which C-O stretching and O-H deformation appear at 1296, 1080, and 1037 cm^{-1}. Finally, N-H stretching appears at 3285 cm^{-1}.

In the ^{1}H-NMR spectrum of L1 (Figure 1) aromatic protons appear at 7.2–7.8 ppm, OH and NH protons appear as a broadened peak at 3.69, the methylene protons of Ar-CH_2-N at 3.54 while those of NCH_2O appear at 3.28 ppm. The ^{13}C-NMR spectrum (Figure S3) shows the aromatic carbons in the range of 128–145 ppm, the C-O carbon at 63, and the quaternary carbon at 60.4 ppm, while the Ar-**C**H_2-N carbon appears at 57 ppm [29].

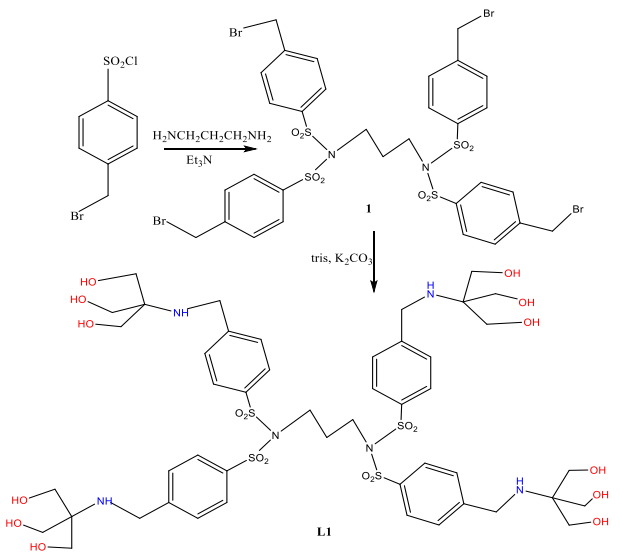

Scheme 1. Synthesis of L1.

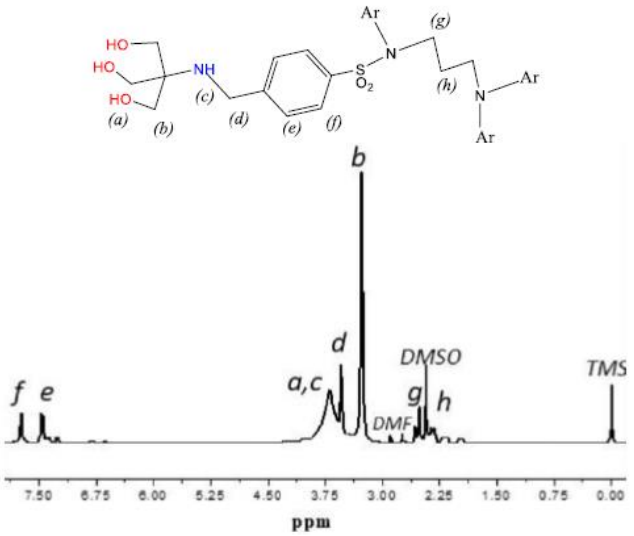

Figure 1. ^{1}H-NMR Spectrum of L1.

3.2. Dendrimers derived from 4-nitrobenzenesulfonyl chloride, L2

L2 was prepared by reacting 1,3-diaminopropane with excess 4-nitrobenzenesulfonyl chloride, followed by reduction with $SnCl_2$ to produce the tetraamine, Compound 3, (Scheme 2). The IR spectrum of the nitro compound, Compound 2, shows the aromatic vibrations at 1606, 1475, and 740 cm^{-1}, and the sulfonyl vibrations at 1311, 1162, and 1115 cm^{-1}. The nitro groups stretching appear at 1527 (strong asymmetric N-O vibration), 1350 (strong symmetric N-O vibration), 854, and 612 cm^{-1} (both bending vibrations) as expected for aromatic nitro compounds. Several changes occur upon reduction to the off-white tetraamine (Figure S4). The N-H stretching frequencies appear at 3454 and 3381 cm^{-1} as expected for aromatic primary amines. NO_2 peaks disappeared.

Compound 3 was then condensed with 4-bromomethylbenzenesulfonyl chloride causing the NH_2 features to disappear, while C-Br stretching appears at 600 cm^{-1}. No frequencies appear in the 3200–3300 cm^{-1} region, proving the attachment of two sulfonyl groups to each nitrogen atom of the primary amine (Figure S5). Reacting the product, Compound 4, with tris produced L2. The IR spectrum of L2 (Figure S6) shows a band at 3420 cm^{-1} due to OH stretching [29]. Coupled C–O stretching and O–H deformation appear at 1085 cm^{-1}. Moreover, in the ^{1}H-NMR spectrum of L2 (Figure S7) the OH protons appear as a broadened peak at 4.34 ppm. The methylene protons of NCH_2Ar appear at 4.49 and those of CH_2O at 3.36 ppm. The ^{13}C-NMR spectrum (Figure S8) shows the aromatic carbons in the range 126–143 ppm, the C-O carbon at 61.7, and the quaternary carbon at 60.6 ppm. Ar-CH_2-N carbons appear at 52.5 ppm.

3.3. Mesitylene-derived dendrimer, L3

Tris(bromomethyl)mesitylene was reacted with tris to afford L3 (Scheme 3). In the ^{1}H-NMR spectrum of L3 (Figure S9) the terminal OH protons appear broadened at 4.41 ppm. The methylene protons of Ar-CH_2-N appear at 3.75, while those of CH_2O at 3.47 ppm. The ^{13}C-NMR spectrum (Figure S10) shows the aromatic carbons at 134.9 and 135.6 ppm, the C-O carbon at 61.6, C-CH_2-N at 40.8, and the CH_3 carbons at 15.2 ppm. The IR spectrum (Figure S11) shows a broad band attributed to OH stretching at 3355 cm^{-1}. Coupled C–O stretching and O–H deformation appear at 1042 and 1346 cm^{-1}.

3.4. Metal complexes of the dendrimers

The dendrimers were reacted at RT separately with the metal ions Fe^{3+}, Al^{3+} (as chlorides), and UO_2^{2+} as the nitrate, in DMF as a solvent. L1 was also reacted with uranyl in HNO_3 to study its ability to bind uranium from acidic solutions. L1 was used in a 1:4 molar ratio to the metals, since it has a capacity of 4 ions/dendrimer molecule, L3 in a 1:3 ratio (capacity of 3), and L2, which has the highest capacity at 8, in a 1:8 ratio. The hard metals form coordinate bonds with the hard oxygen atoms on the periphery of the dendrimers (Figure 2). The Fe complexes of the dendrimers have brown colors, Al complexes off-white, and UO_2^{2+} complexes yellow, as expected from the coordination to OH [27]. The complexes decomposed at 240–270 °C. The complexes were slightly soluble in the polar solvents DMF, DMSO, and water and insoluble in the less polar Et_2O and ethyl acetate. Complexes with L2 were the least soluble in water, a direct result of the large size of the dendrimer. Complexation was studied by IR and UV-Vis spectroscopy as well as TGA. Elemental analysis confirmed the composition of the complexes.

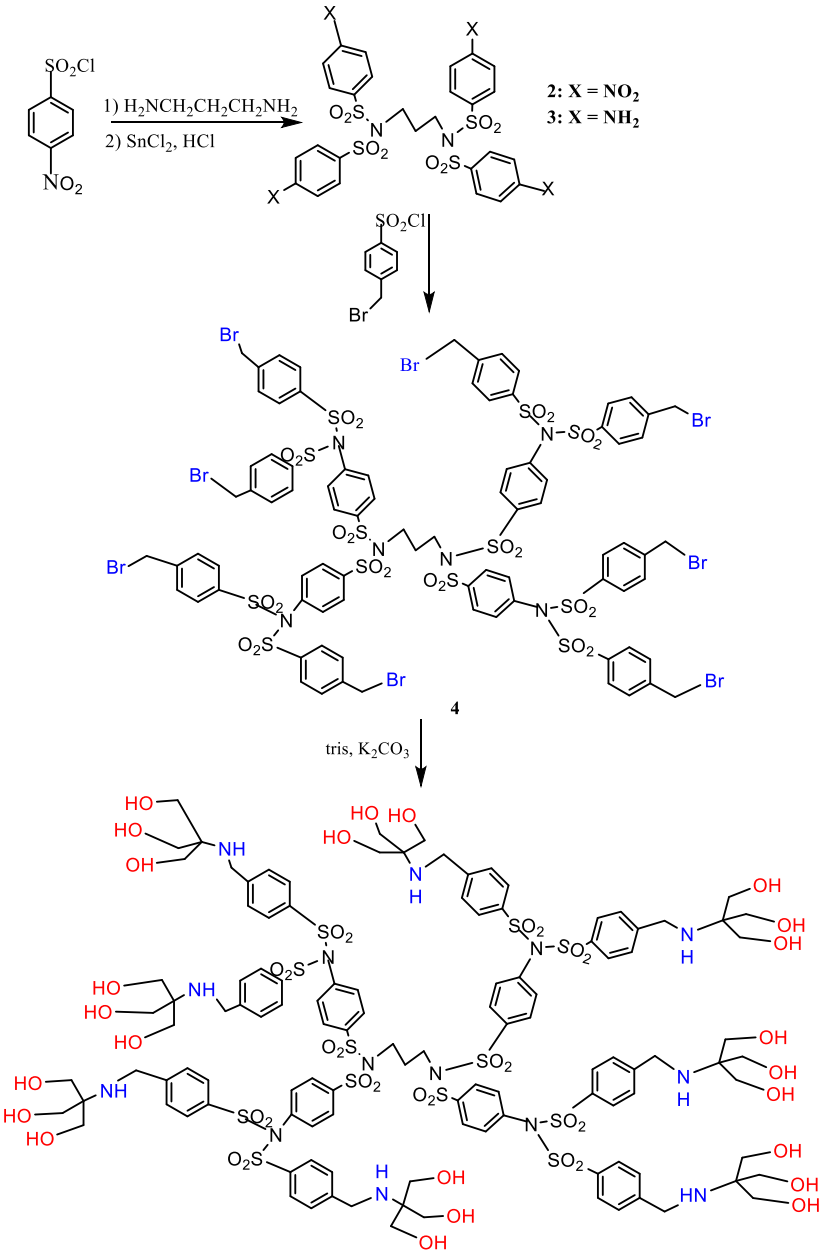

Scheme 2. Synthesis of L2.

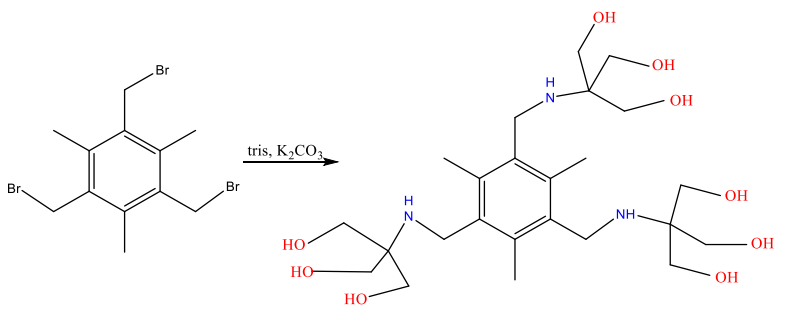

Scheme 3. Synthesis of L3.

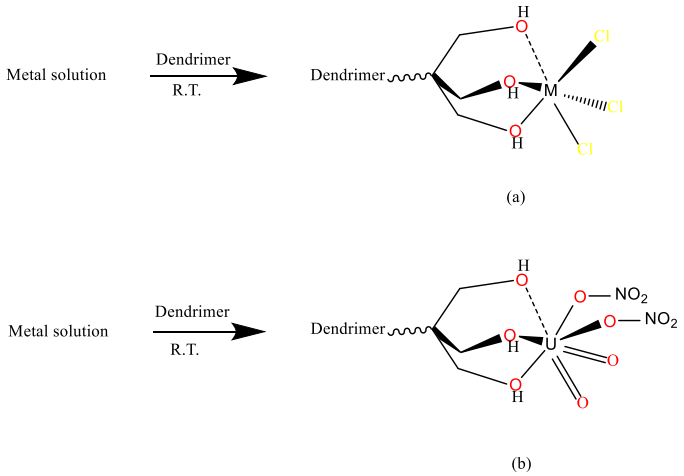

Figure 2. Binding of the dendrimers to the metal ions. M = Fe, Al.

Thermal gravimetric analysis

TGA data of the metal complexes are given in Table 1. The detailed fragmentation patterns and the assignments of the fragments lost from the peripheral groups, the branches, and the core, as well as the residues formed all comply with the proposed structures of the dendrimers and their metal complexes. Fragmentation starts with the loss of bound DMF followed by alcohol moieties from the OH terminals and then the amine branches. The loss of benzenesulfonyl fragments leaves the metal salt behind [30].

The complexes have bound DMF as indicated by the high temperature at which DMF leaves (from about 140 °C and up to 300 °C in some complexes) and the mass percent of the residues [31]. Decomposition of all complexes started at 250–325 °C. Decomposition of the ligand in L1Fe_4Cl_{12}•4DMF (Figure S12) started with the loss of CH_3OH from the terminals and $(CH_3)_2NH$ from the branches and continued till the formation of the residue, which forms 20% of the complex (calc. 20.68%) [32].

A uranyl nitrate residue forms 47.9% of the complex L2$U_8O_{16}(NO_3)_{16}$•8DMF (Figure 3). Decomposition of the ligand started by losing CH_3OH from the termini and ended at 850 °C [32]. Meanwhile, the ligand in L2Fe_8Cl_{24}•8DMF started decomposing by losing tris moieties and continued till an inorganic residue formed (Figure S13). The residue forms 34.0% of the complex L3Al_3Cl_9•3DMF (Figure S14) and 60.7% of L3$U_3O_6(NO_3)_6$•3DMF, where the ligand started decomposing by losing terminal tris and ended with the loss of benzene from the interior (Figure S15). On the other hand, the decomposition of the ligand in L3Fe_3Cl_9•3DMF (Figure S16) started with the loss of terminal CH_3OH and continued till the formation of $FeCl_2$ (29.5% of the complex).

IR spectra

The IR spectra of the Fe complexes (Figure 4, Figure S17) show shifts in the stretching vibration of the O–H groups and the coupled O–H deformation and C–O stretching vibrations compared to the free dendrimers (Table 2). These shifts together with the appearance of a new peak in the complexes in the 500–600 cm^{-1} range are attributed to the newly formed Fe–O bonds, proving that the binding of Fe takes place at the terminal OH groups of the dendrimers [33].

Diallo et al. observed significant binding of UO_2^{2+} to PAMAM dendrimers in solutions containing up to 1.0 M HNO_3 and H_3PO_4 [7]. The IR spectra of the U complexes (Figure S18) prove the binding of UO_2^{2+} ions from the solutions to OH with shifts to different frequencies for the OH stretching vibrations compared to the free dendrimers (Table 2). This is supported by the altered intensity and shift of the coupled C–O stretching and O–H deformation and the appearance of new peaks at 645–500 cm^{-1} due to UO_2^{2+}-O single bonds [34]. The absorption at 925–825 cm^{-1} is typical of UO_2^{2+} [35]. The peaks at 1500–1560 cm^{-1} and 1300–1355 cm^{-1} are due to coordinated nitrate [36]. The nitric acid solution was evaporated over several days thus reflecting the stability of these dendrimers in acidic solutions and showing their potential for binding metals from acidic solutions.

The IR spectrum of the Al complex L1Al showed notable changes from the free ligand spectrum (Figure S19). Although C-O stretching and O-H deformation of the OH groups appear at 1298 and 1039 cm^{-1}, close to the ligand positions (1296 and 1037), the absorption at 3335 cm^{-1} disappears. Thus, the involvement of OH groups in Al binding cannot be excluded, although they may be deprotonated. This suggestion is supported by the appearance of a new peak at 592 cm^{-1}, which

Table 1. TGA of the complexes.

Complex	Temperature (°C)	Mass loss (%) (Remaining)	Decomposition assignment (Calc. Mass %)
L1Fe_4Cl_{12}•4DMF ($C_{59}H_{98}N_{10}O_{24}S_4Fe_4Cl_{12}$)	180–280	24.0 (73.0)	Loss of 4 DMF, 8 CH_3OH (74.0)
	280–600	15.0 (58.0)	Loss of 4 CH_3OH, 4 $(CH_3)_2NH$ (59.3)
	600–760	26.0 (32.0)	Loss of 4 $C_6H_4SO_2$ (32.5)
	760–850	12.0 (20.0)	Residue, Fe_4Cl_6 (20.7)
L2$U_8O_{16}(NO_3)_{16}$•8DMF($C_{139}H_{206}N_{38}O_{120}S_{12}U_8$)	160–290	13.1 (86.9)	Loss of 8 DMF, 8 CH_3OH (87.3)
	290–580	22.4 (64.5)	Loss of 8 C_6H_4-$C_4H_9NO_2$ (65.6)
	580–735	7.7 (56.8)	Loss of 4 $N(SO_2)_2$ (56.2)
	735–850	8.9 (47.9)	Residue, $U_8O_{16}(NO_3)_{16}$ (47.6)
L2Fe_8Cl_{24}•8DMF ($C_{139}H_{206}N_{22}O_{56}S_{12}Fe_8Cl_{24}$)	160–300	13.1 (86.9)	Loss of 8 DMF (87.7)
	300–600	21.9 (65.0)	Loss of 8 $C_5H_{11}NO_3$ (65.3)
	600–785	26.5 (38.5)	Loss of 4 $N(SO_2C_6H_5)_2$ (39.2)
	785–850	18.5 (20.0)	Residue, Fe_8Cl_{16} (21.3)
L3Al_3Cl_9•3DMF ($C_{33}H_{66}N_6O_{12}Al_3Cl_9$)	160–280	19.8 (80.2)	Loss of 3DMF (80.7)
	280–510	35.3 (44.9)	Loss of 3 $C_5H_{13}NO_3$ (45.1)
	510–850	10.9 (34.0)	Residue, Al_3Cl_9 (35.1)
L3$U_3O_6(NO_3)_6$•3DMF ($C_{33}H_{66}N_{12}O_{36}U_3$)	140–850	39.3 (60.7)	Loss of 3 DMF, 3 $C_5H_{13}NO_3$, 3 CH_3, C_6H_6, Residue of $U_3O_6(NO_3)_6$ (61.5)
L3Fe_3Cl_9•3DMF ($C_{33}H_{66}N_6O_{12}Fe_3Cl_9$)	140–240	18.0 (82.0)	Loss of 3 DMF (82.1)
	240–400	15.0 (67.0)	Loss of 3 C_2H_6 and 3 CH_3OH (66.6)
	400–600	19.0 (48.0)	Loss of $C_6H_6N_3O_6$ (49.0)
	600–780	18.5 (29.5)	Residue, Fe_3Cl_6 (30.0)

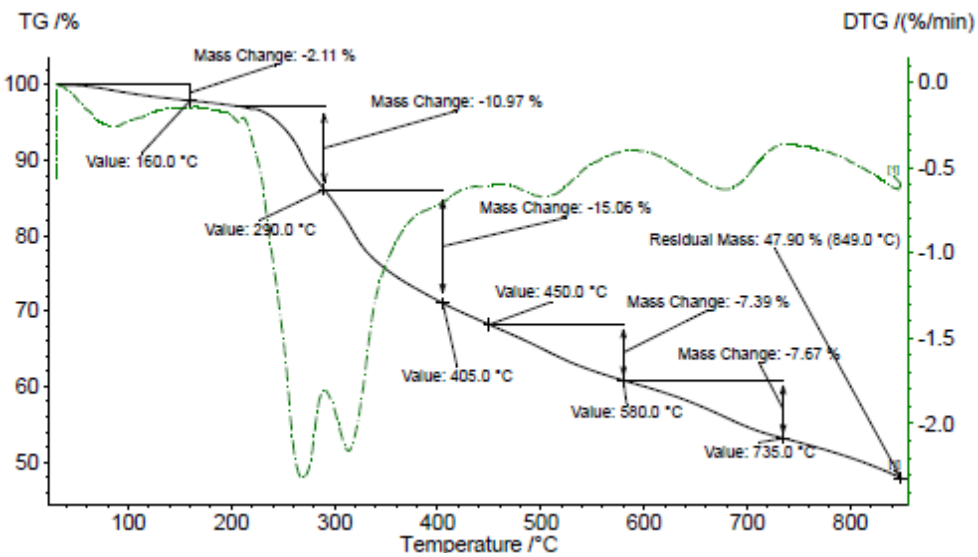

Figure 3. TGA and differential thermogravimetry (DTG) curves of L2$U_8O_{16}(NO_3)_{16}$•8DMF.

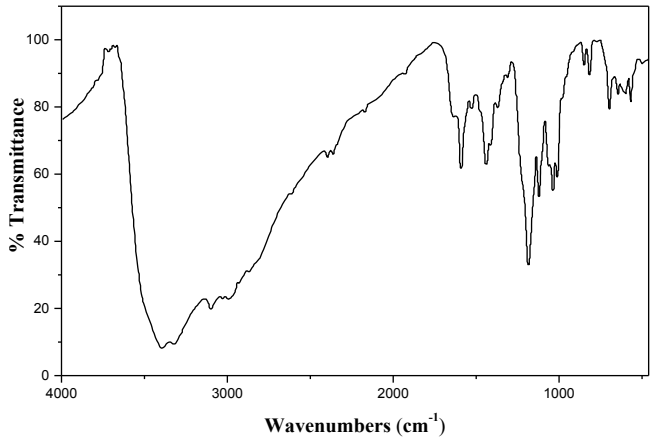

Figure 4. The IR Spectrum of the Fe complex of L2.

Table 2. IR data of the uranium and iron complexes.

Vibration	Peak (cm^{-1})					
	FeL1	FeL2	FeL3	UL1	UL2	UL3
O-H stretching	3234	3390	3405	3449	3330	3342
C-O stretching and O-H deformation	1296, 1058, 1037	1040	1330, 1084	1391, 1023	1384, 1044	1383, 1066
$\nu_{(M-O)}$	595	571	550	500	645, 576	532
$\nu_{(U=O)}$	-	-	-	826	924	927
DMF $\nu_{(C=O)}$	1630	1635	1627	1618	1631	1653
NO_3^- vibrations, (asymm., symm.)	-	-	-	1525, 1300	1504, 1344	1561, 1355

is assigned to the Al-O stretching frequency. Finally, the spectrum indicates the presence of DMF in the complex due to the presence of absorptions at 1664 and 3073 cm^{-1}. The IR spectra of Al^{3+} with L2 and L3 (Figure S20) do not show recognizable features that suggest Al binding to L2 or L3.

UV-visible spectra

UV-visible spectra were recorded for the complexed dendrimers in aqueous solutions and compared to those of the free ligands as well as those of the aqueous ions. No absorptions were observed for the free L1 and L3 (Figures S21 and 5, respectively).

New ligand-to-metal charge transfer (LMCT) peaks were observed at 300 nm for the Al-complexed dendrimers L1 and L3. These absorptions were not observed in the spectra of the free ligands or Al^{3+} ions. On the other hand, the Cl → Fe^{3+} CT absorptions were shifted from 334 nm in $FeCl_3$ [37] to 301 nm upon complexation of Fe to L3, and 300 nm upon Fe binding to L1, which is in the range expected of the O → Fe^{3+} charge transfer in Fe^{3+}-OH moieties [38]. The extinction coefficient reported here (ε, 3.16×10^3 $M^{-1}cm^{-1}$ for L1Fe and 1.58×10^3 for L3Fe) is similar to previous reports [38].

The UV-vis spectrum of the dendrimer L2 has a peak with a maximum at 296 nm (ε, 6.21×10^3) due to n → π* transitions (Figure S22). The spectra of the Al and Fe complexes of L2 have peaks at 304 and 300 nm, respectively. These strong absorptions can be attributed to oxygen → metal LMCT.

O → U LMCT from the ligand-based orbitals σ_u and π_u to the metal-based orbitals δ_u and φ_u appear at 370 and 415 nm in free uranyl nitrate [39]. The absorptions are not strong since they are Laporte-forbidden [40]. These absorptions become much stronger and appear to shift to new positions at 300, 357, and 429 nm (Figure S21) upon forming L1U. Similar peaks were obtained for L2U at 297, 351, and 434 (Figure S22) and L3U at 302, 382, and 430 nm (Figure 5).

These results from the electronic spectra give further proof to conclusions drawn from the results obtained using the previous techniques that the metal ions are bound to the hydroxyl terminal groups of the dendrimers (Figure 2).

3.5. Selective binding of iron from aluminum solutions

The dendrimers were tested for their ability to separate Fe^{3+} from Al^{3+} by adding each dendrimer, separately, to solutions containing equal amounts of both metal ions. The metals were added such that the concentration of each one would be enough to fulfill the capacity of the dendrimer by itself in order to get a clear answer to the question of the dendrimers' selectivity toward Fe^{3+} and Al^{3+}. Fe^{3+} concentration was determined spectrophotometrically using NaSCN as a complexing agent, whereas Al^{3+} was tested using the Aluminon test. While the Aluminon tests were all positive and proved the presence of significant amounts of Al in all samples, the concentration of free Fe ions was found to be lowered to less than 1% of its original value in all three tests (Table 3). Solution 2 did not produce any detectible quantities of Fe using the same test.

These experiments give proof of the selectivity of these OH-terminated dendrimers toward the Fe^{3+} ions compared to the Al^{3+} ions and therefore could work to bind Fe selectively from Al solutions. Moreover, the quantitative binding of Fe from the solution gives further proof of the loading capacity of these dendrimers, i.e. L1 binds 4 Fe^{3+} ions, L2 binds 8, and L3 binds 3 ions. L2 in particular shows the most promise for separating Fe from Al because of the low solubility of its Fe complex in water which facilitates its separation from Al, and because of its higher loading capacity.

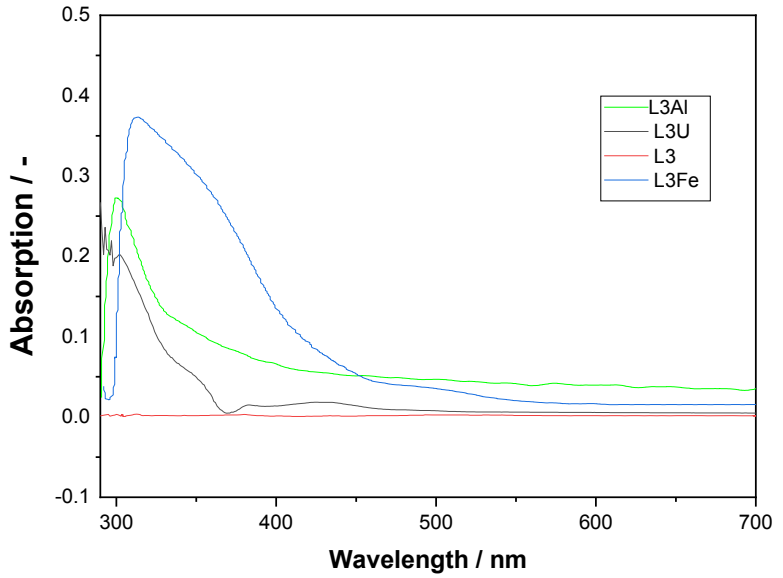

Figure 5. UV-Vis spectra of L3 and its complexes.

Table 3. Selective binding of Fe^{3+} in solutions of Fe^{3+} and Al^{3+}.

Dendrimer	Original Fe^{3+} conc. (M)[a]	Final Fe^{3+} conc. (M)[b]	Free Fe^{3+} left (%)
L1	1.26×10^{-2}	3.00×10^{-5}	2.40×10^{-1}
L2	3.70×10^{-3}	0.00	0.00
L3	2.33×10^{-2}	3.96×10^{-5}	1.70×10^{-1}

a. Concentration before adding the dendrimer. b. Concentration after adding the dendrimer.

4. Conclusions

The dendrimers prepared form an addition to the family of dendritic molecules and have the ability to bind to many metals of industrial significance. The composition and structure of the products were proved by different spectroscopic methods, elemental analysis, and TGA. The TGA fragmentation patterns of the complexes and their assignments all comply with the proposed structures of the dendrimers and their complexes. The dendrimers bind the metals studied although they do not appear to bind Al strongly. The experiments performed with mixtures of Fe and Al show a strong preference of these dendrimers toward the Fe^{3+} ions over the Al^{3+} ions, and therefore could potentially separate Fe from Al solutions. The dendrimers also appear suitable for binding UO_2^{2+} from acids and show high stability over several days.

Acknowledgments

We would like to thank Abdul Hameed Shoman Foundation for funding (grant 3/2013).

Supplementary material

This file includes Figures of the IR, ^{1}H-NMR, ^{13}C-NMR, and UV-Vis spectra as well as TGA of the compounds not shown in the main text.

References

[1] Daniel Luis PH, Marcos MG. Dendrimer Applications: A Brief Review. Current Organic Chemistry 2021; 25. https://doi.org/10.2174/1385272825666210525155816

[2] Wang XQ, Li WJ, Wang W, Yang HB. Rotaxane Dendrimers: Alliance between Giants. Accounts of Chemical Research 2021; 54: 4091-4106. https://doi.org/10.1021/acs.accounts.1c00507

[3] Ebrahimi R, Hayati B, Rezaee R, Shahmoradi B, Safari M et al. Adsorption of cadmium and nickel from aqueous environments using a dendrimer. Journal of Advances in Environmental Health Research 2020; 8: 19-24. https://doi.org/10.22102/jaehr.2020.128442.1075

[4] Gajjar D, Patel R, Patel H, Patel PM. Removal of heavy metal ions from water by Hydroxyl terminated Triazine-based Dendrimer. Desalination and Water treatment 2015; 55: 1209-1219. https://doi.org/10.1080/19443994.2014.922446

[5] Iannazzo D, Pistone A, Ziccarelli I, Espro C, Galvagno S et al. Removal of heavy metal ions from wastewaters using dendrimer-functionalized multi-walled carbon nanotubes. Environmental Science and Pollution Research International 2017; 24: 14735–14747. https://doi.org/10.1007/s11356-017-9086-2

[6] Wu Y, Bai H, Zhou Q, Li S, Tong Y et al. Preparation of Polyamidoamine Dendrimer Modified Magnetic Nanoparticles and Its Application for Reliable Measurement of Sudan Red Contaminants in Natural Waters at Parts-Per-Billion Levels. Frontiers in Chemistry 2021; 9: 708995. https://doi.org/10.3389/fchem.2021.708995

[7] Diallo MS, Arasho W, Johnson Jr JH, Goddard III WA. Dendritic Chelating Agents. 2. U(VI) Binding to Poly(amidoamine) and Poly(propyleneimine) Dendrimers in Aqueous Solutions. Environmental Science & Technology 2008; 42: 1572-1579. https://doi.org/10.1021/es0715905

[8] Guzmán L, Durán Lara EF, Donoso W, Nachtigall FM, Santos LS. In Vivo Nanodetoxication for Acute Uranium Exposure. Molecules 2015; 20: 11017-11033. https://doi.org/10.3390/molecules200611017

[9] Chauhan AS. Dendrimers for Drug Delivery. Molecules 2018; 23: 938. https://doi.org/10.3390/molecules23040938

[10] Abd El Aziz AS, Abdelghani AA, El Ghezlani EG, Abou El ezz D, Abdel Rahman LH. Pharmacological Evaluation of Novel Organoiron Dendrimers as Antimicrobial and Anti-Inflammatory Agents. Macromolecular Bioscience 2021; 21: 2000242. https://doi.org/10.1002/mabi.202000242

[11] Yao Q, Chen H, Huang H, Liu B. Mechanism and effect of hydroxyl-terminated dendrimer as excellent chrome exhausted agent for tanning of pickled pelt. Journal of Cleaner Production 2018; 202: 543-552. https://doi.org/10.1016/j.jclepro.2018.08.164

[12] Appelhans D, Oertel U, Mazzeo R, Komber H, Hooffmann J et al. Dense-shell glycodendrimers: UV/Vis and electron paramagnetic resonance study of metal ion complexation. Proceedings of the Royal Society A 2010; 466: 1489–1513. https://doi.org/10.1098/rspa.2009.0107

[13] Cusnir R, Imberti C, Hider RC, Blower PJ, Ma MT. Hydroxypyridinone Chelators: From Iron Scavenging to Radiopharmaceuticals for PET Imaging with Gallium-68. International Journal of Molecular Sciences 2017; 18: 116. https://doi.org/10.3390/ijms18010116

[14] Ye J, Abiman P, Crossley A, Jones JH, Wildgoose GG et al. Building Block Syntheses of Gallic Acid Monomers and Tris-(O-gallyl)-gallic Acid Dendrimers Chemically Attached to Graphite Powder: A Comparative Study of Their Uptake of Al(III) Ions. Langmuir 2010; 26: 1776-1785. https://doi.org/10.1021/la902497s

[15] Zhoua T, Winkelmannb G, Daia ZY, Hider RC. Design of clinically useful macromolecular iron chelators. Journal of Pharmacy and Pharmacology 2011; 63: 883–892. https://doi.org/10.1111/j.2042-7158.2011.01267.x

[16] Carta F, Osman SM, Vullo D, AlOthman Z, Supuran CT. Dendrimers incorporating benzenesulfonamide moieties strongly inhibit carbonic anhydrase isoforms I-XIV. Organic & Biomolecular Chemistry 2015; 13: 6453-7. https://doi.org/10.1039/c5ob00715a

[17] Khanam S, Rai SK, Tewari AK. Advancement in the sulfone-based dendrimers: From synthesis to application. Advanced Materials Letters 2017; 8: 1005-1019. https://doi.org/10.5185/amlett.2017.1609

[18] Singh P. Synthesis of mesitylene-based polyamine dendrimer for functionalisation of single-walled carbon nanotubes. Journal of Experimental Nanoscience 2015; 10: 429–437. https://doi.org/10.1080/17458080.2013.840935

[19] Habashi F. Textbook of Hydrometallurgy. Second ed. Quebec, Canada: Metallurgie Extractive Quebec, 1999.

[20] Mishra RK, Rout PC, Sarangi K, Nathsarma KC. A comparative study on extraction of Fe(III) from chloride leach liquor using TBP, Cyanex 921 and Cyanex 923. Hydrometallurgy 2010; 104: 298-303. https://doi.org/10.1016/j.hydromet.2010.07.003

[21] Li M, He Z, Zhou L. Removal of iron from industrial grade aluminum sulfate by primary amine extraction system. Hydrometallurgy 2011; 106: 170-4. https://doi.org/10.1016/j.hydromet.2010.12.018

[22] Stefanakis MI, Monhemius AJ. Determination of organic phase complexes formed on extraction of iron(III) from aluminium nitrate solutions with versatic 10. Hydrometallurgy 1985; 15: 113-139. https://doi.org/10.1016/0304-386X(85)90070-2

[23] Beltrami D, Cote G, Mokhtari H, Courtaud B, Moyer BA et al. Recovery of Uranium from Wet Phosphoric Acid by Solvent Extraction Processes. Chemical Reviews 2014; 114: 12002–12023. https://doi.org/10.1021/cr5001546

[24] Singh DK, Mondal S, Chakravarty JK. Recovery of Uranium from Phosphoric Acid: A Review. Solvent Extraction and Ion Exchange 2016; 34: 201-225. https://doi.org/10.1080/07366299.2016.1169142

[25] Lu X, Zhang D, Reda AT, Liu C, Yang Z et al. Synthesis of Amidoxime-Grafted Activated Carbon Fibers for Efficient Recovery of Uranium(VI) from Aqueous Solution. Industrial & Engineering Chemistry Research 2017; 56: 11936-11947. https://doi.org/10.1021/acs.iecr.7b02690

[26] Cotton S. Lanthanide and Actinide Chemistry. NY, USA: Wiley, 2006.

[27] Greenwood NN, Earnshaw A. Chemistry of the Elements. Second ed. Burlington, MA, USA: Elsevier, B/H, 2006.

[28] Szabo Z, Toraishi T, Vallet V, Grenthe I. Solution chemistry of actinides: Thermodynamics, structure and reaction mechanisms. Coordination Chemistry Reviews 2006; 250: 784–815. https://doi.org/10.1016/j.ccr.2005.10.005

[29] Kemp W. Organic Spectroscopy. Third ed. Hong Kong: EL/BS with Macmillan, 1991.

[30] Vardareli TK, Keskin S, Usanmaz A. Thermal Degradation of Poly(Allyl Methacrylate) by Mass Spectroscopy and TGA. Journal of Macromolecular Science, Part A: Pure and Applied Chemistry 2006; 43 (10): 1569-1581. https://doi.org/10.1080/10601320600896900

[31] Firuzabadi FD, Asadi Z, Yousefi R. Synthesis of new Nano Schiff Base Complexes: X-Ray Crystallography, Thermal, Electrochemical and Anticancer Studies of Nano Uranyl Schiff Base Complexes. Bulletin of the Chemical Society of Ethiopia 2018; 32: 89-100. https://doi.org/10.4314/bcse. v32i1.8

[32] Çılgı GK, Cetişli H, Donat R. Thermal and kinetic analysis of uranium salts. Part III. Uranium(IV) oxalate hydrates. Journal of Thermal Analysis and Calorimetry 2014; 115: 2007–2020. https://doi.org/10.1007/s10973-013-3341-7

[33] Nagajothi A, Kiruthika A, Chitra S, Parameswari K. Fe(III) Complexes with Schiff base Ligands : Synthesis, Characterization, Antimicrobial Studies. Research Journal of Chemical Sciences 2013; 3: 35-43.

[34] Shundalau MB, Zazhogin AA, Zazhogin AP, Komyak AI, Umreiko DS. Structure and Vibrational Spectra of Uranyl Dinitrate Complexes with Water and DMSO. Journal of Applied Spectroscopy 2014; 82: 25-32. https://doi.org/10.1007/s10812-015-0059-2

[35] Nakamoto K. Infrared Spectra of Inorganic and Coordination Compounds. Fourth ed. NY, USA: Wiley, 1996.

[36] Bullock JI. Infrared Spectra of Some Uranyl Nitrate Complexes. Journal of Inorganic and Nuclear Chemistry 1967; 29: 2257-2264. https://doi.org/10.1016/0022-1902(67)80280-X

[37] Abderrazak H, Dachraoui M, Lendl B. A Novel Flow Injection Procedure for Determination of Phosphate in Industrial Raw Phosphoric Acid. Analyst 2000; 125: 1211-1213. https://doi.org/10.1039/b001208o

[38] Turner RC, Miles KE. The Ultraviolet Absorption Spectra of the Ferric Ion and its First Hydrolysis Product in Aqueous Solutions. Canadian Journal of Chemistry 1957; 35: 1002-1009. https://doi.org/10.1139/v57-137

[39] Li Y, Su J, Mitchell E, Zhang G, Li J. Photocatalysis with visible-light-active uranyl complexes. Science China Chemistry 2013; 56 (12): 1671-1681. https://doi.org/10.1007/s11426-013-4965-y

[40] Suleimenov OM, Seward TM, Hovey JK. A Spectrophotometric Study on Uranyl Nitrate Complexation to 150 ^{o}C. Journal of Solution Chemistry 2007; 36: 1093-1102. https://doi.org/10.1007/s10953-007-9175-9

Supplementary material

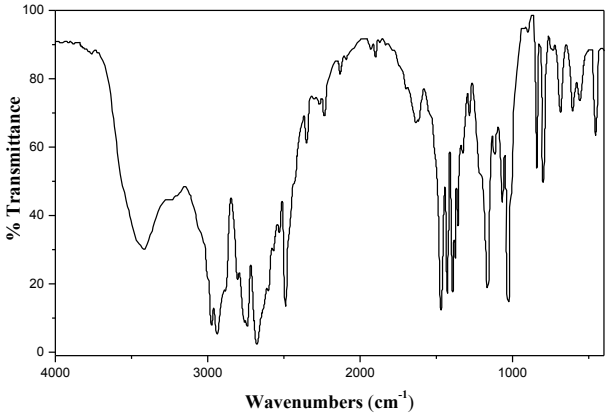

Figure S1. IR spectrum of compound 1.

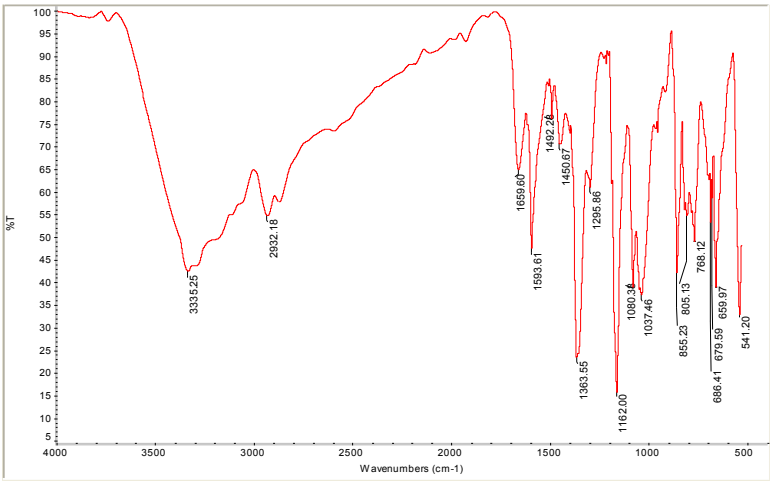

Figure S2. IR spectrum of L1.

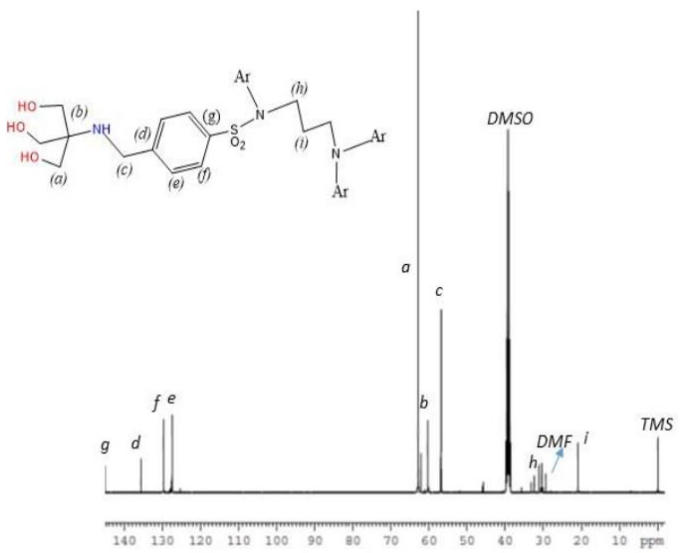

Figure S3. ^{13}C-NMR spectrum of L1.

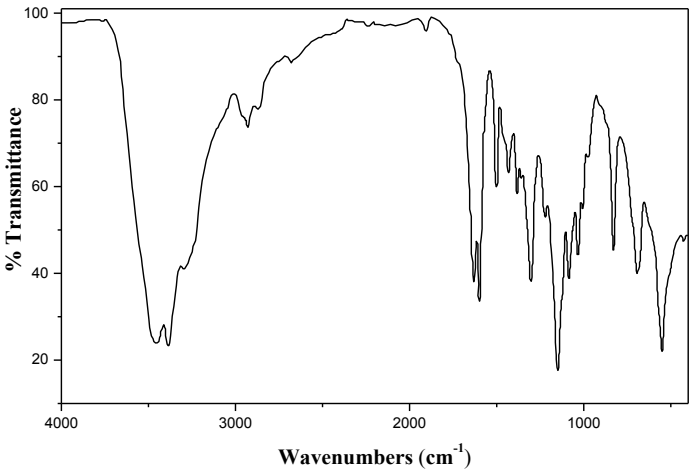

Figure S4. IR spectrum of compound 3.

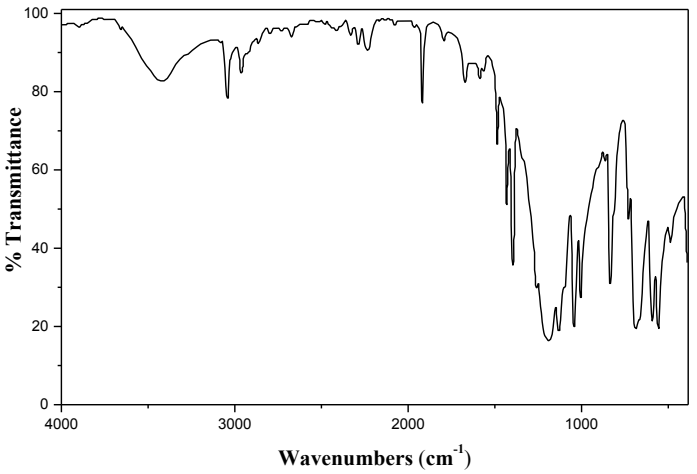

Figure S5. IR spectrum of compound 4.

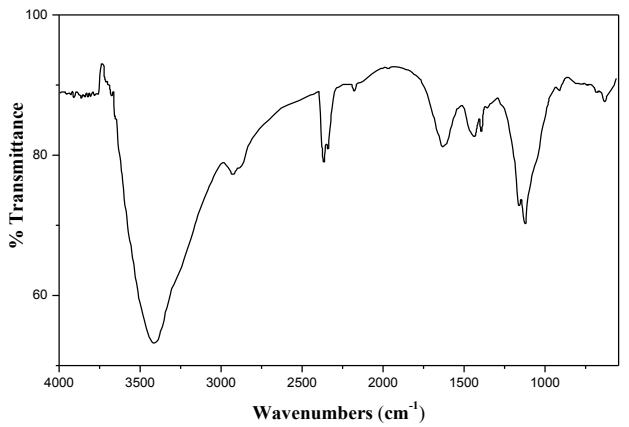

Figure S6. IR Spectrum of L2.

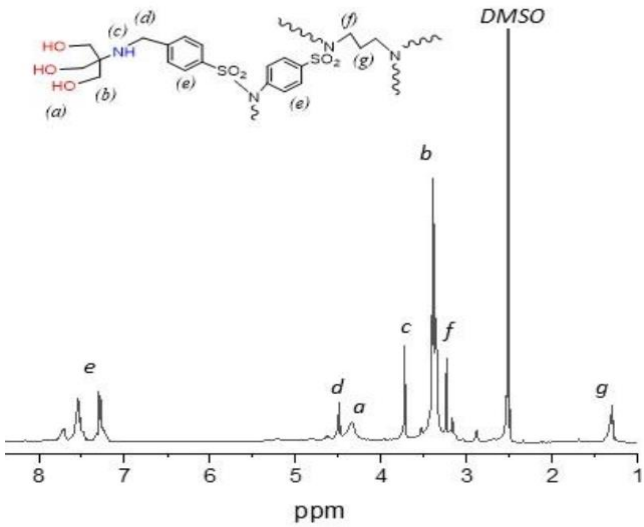

Figure S7. [1]H-NMR spectrum of L2.

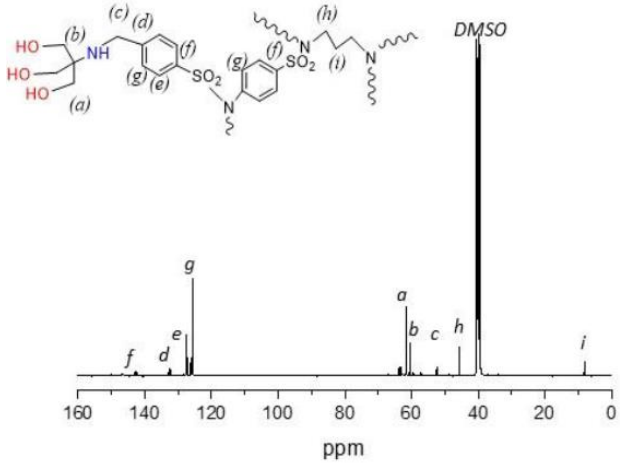

Figure S8. [13]C-NMR spectrum of L2.

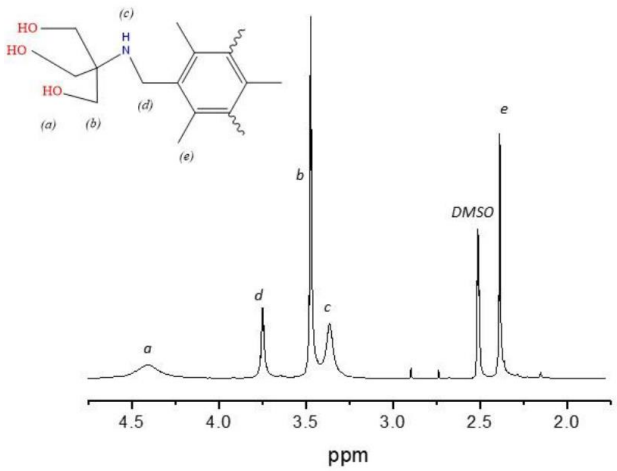

Figure S9. [1]H-NMR spectrum of L3.

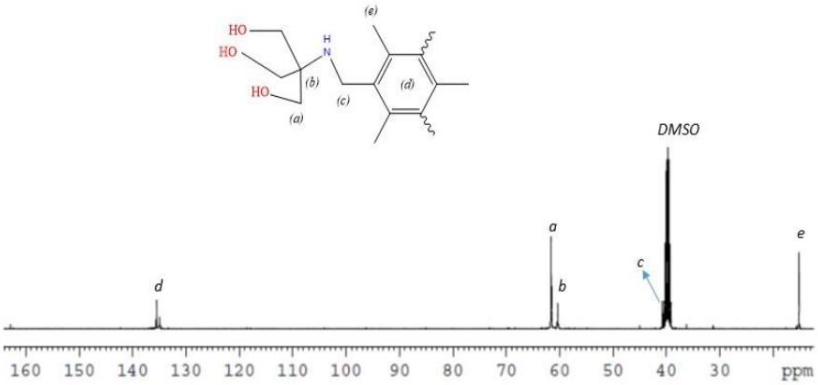

Figure S10. ^{13}C-NMR spectrum of L3.

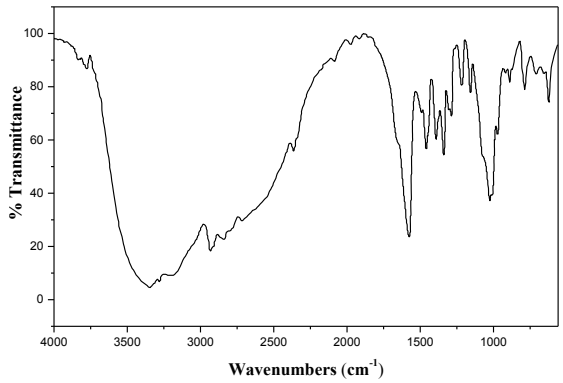

Figure S11. IR spectrum of L3.

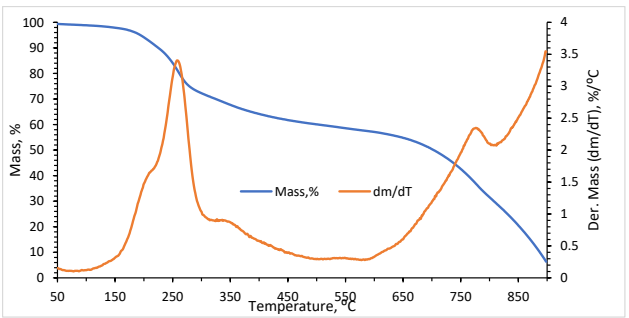

Figure S12. TGA and DTG curves of L1Fe_4Cl_{12}•4DMF.

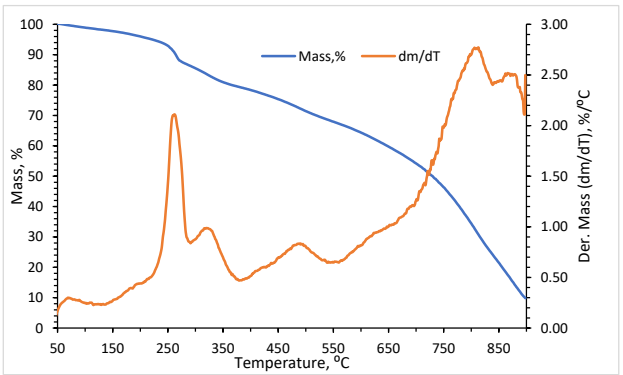

Figure S13. TGA and DTG curves of L2Fe_8Cl_{24}•8DMF.

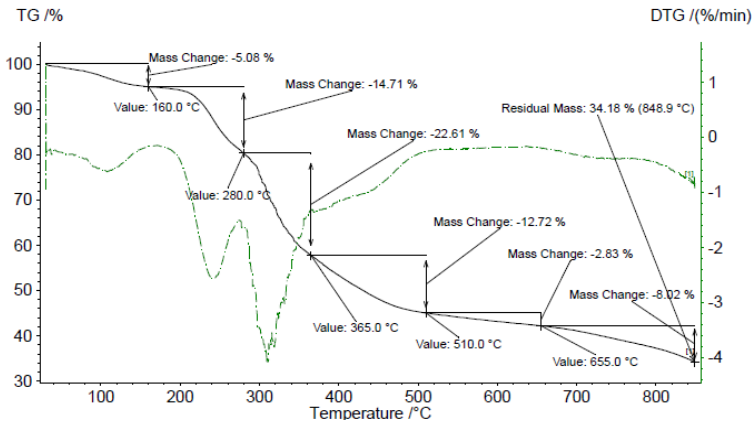

Figure S14. TGA and DTG curves of $L3Al_3Cl_9$•3DMF.

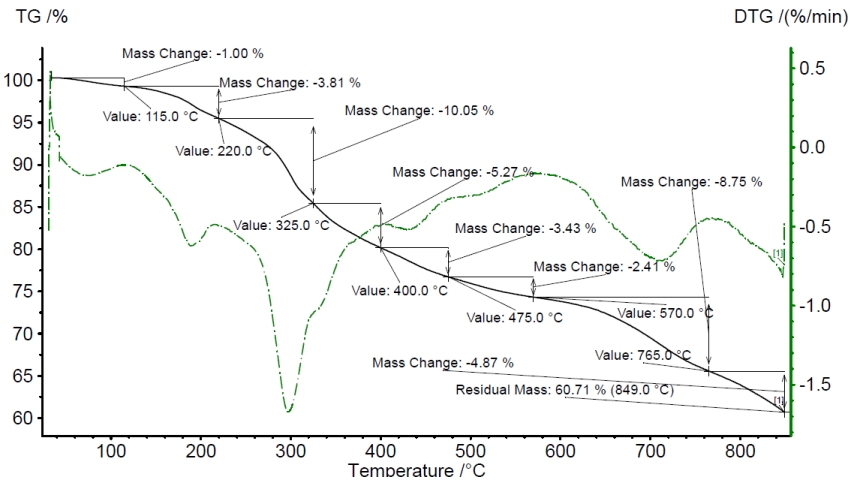

Figure S15. TGA and DTG curves of $L3U_3O_6(NO_3)_6$•3DMF.

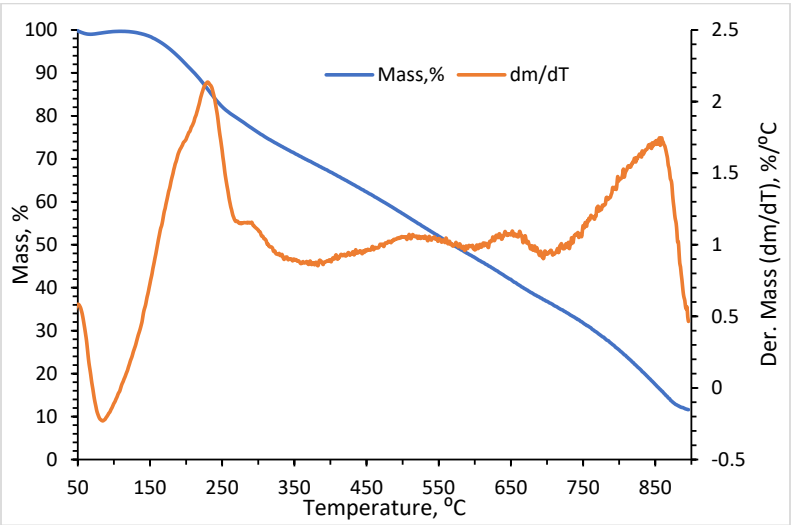

Figure S16. TGA and DTG curves of $L3Fe_3Cl_9$•3DMF.

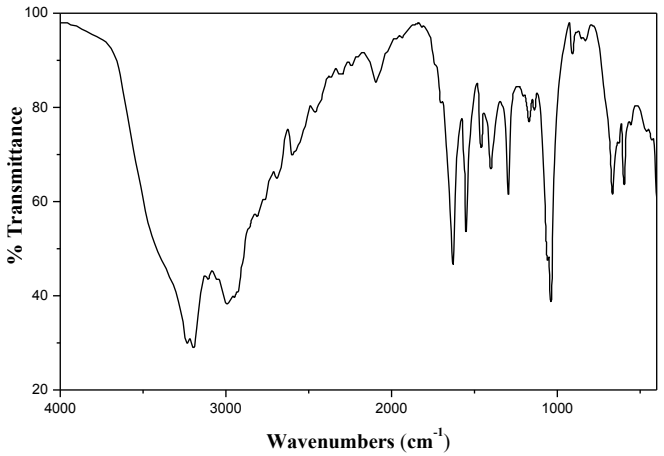

Figure S17. IR spectrum of L1Fe.

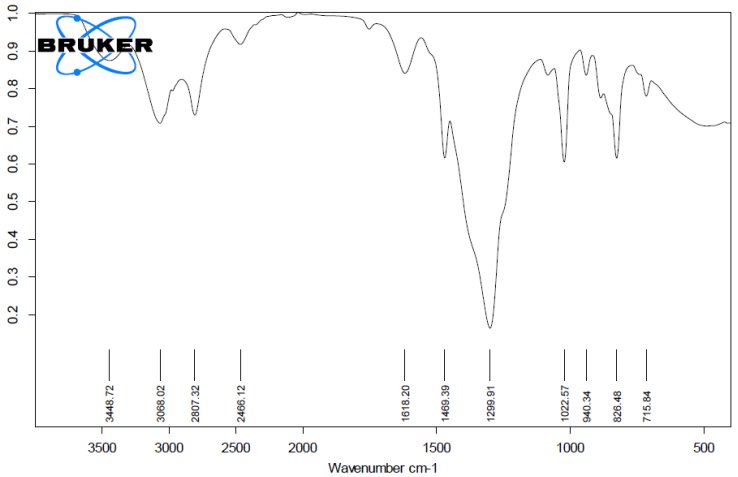

Figure S18. IR spectrum of L1U.

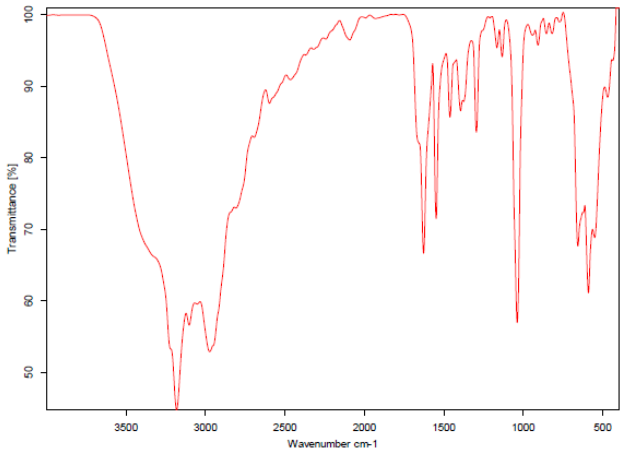

Figure S19. IR spectrum of L1Al.

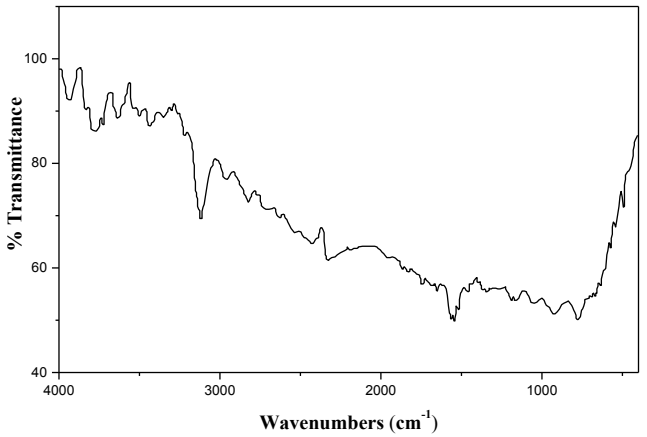

Figure S20. IR spectrum of L2Al.

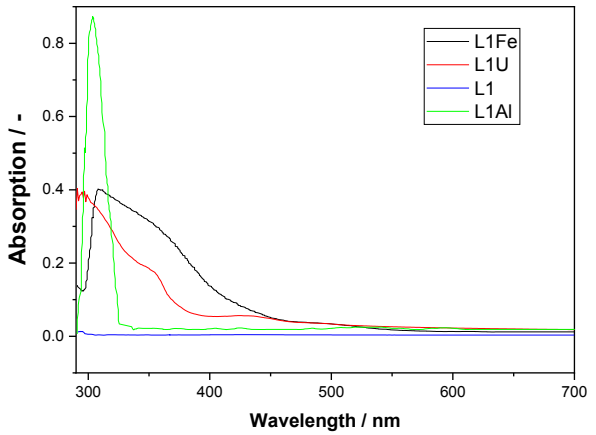

Figure S21. UV-Vis spectra of L1 and its complexes.

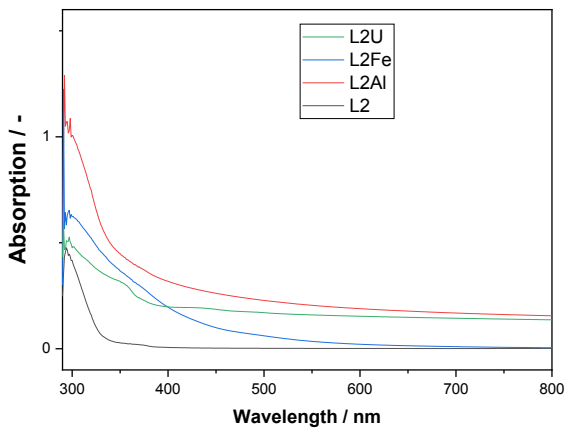

Figure S22. UV-Vis spectra of L2 and its complexes.